Stanford Exploration Project, Report 79, November 16, 1997, pages 169–186

AVO analysis of methane hydrate seismic data

Christine Ecker and David Lumley[1]

keywords: *impedance, amplitudes, AVO, gas, velocity, NMO, sediment*

ABSTRACT

Marine seismic data from the Blake Outer Ridge offshore Florida show strong "bottom simulating reflections" (BSRs) associated with methane hydrate occurrence in deep marine sediments. We use a detailed amplitude versus offset (AVO) analysis of these data to explore the validity of two models regarding the origin of bottom simulating reflectors. After careful preprocessing steps including source wavelet deconvolution, nonlinear trace interpolation, amplitude and moveout traveltime calibration, and velocity analysis, we estimate the P and S impedance contrasts at all subsurface positions. This is done by applying a least-squares elastic parameter inversion method to the preprocessed CMP gathers. Our results suggest that the Blake Outer Ridge BSR is compatible with a model of methane hydrate in sediment, overlying a layer of free methane gas-saturated sediment.

INTRODUCTION

Seismic reflections that parallel the seafloor at subbottom depths of several hundred meters, so called bottom simulating reflectors (BSR), appear to be associated with the base of the stability field for methane hydrates. As methane hydrates contain more potential fuel energy than is present in conventional oil, gas, and coal deposits, they might be an important future energy resource (Kvenvolden, 1993). Therefore, a good understanding of the origin, characteristics and material properties of the bottom simulating reflectors is essential. Only limited information on the nature of the hydrate and the BSRs is available from deep-sea drilling. The risk of heating and destabilizing the initial hydrate conditions during the process of drilling is considerably high. Thus, the core samples and well-logs do not necessarily reflect the correct hydrate characteristics and properties. Therefore, most information must be inferred remotely from seismic reflection data (Hyndman and Davis, 1992; Hyndman and Spence, 1992; Miller et al., 1991; Shipley et al., 1979; Singh et al., 1993). The results of these previous investigations, based mainly on AVO responses and synthetic modeling, indicate that BSRs are characterized by large negative reflection coefficients

[1]**email:** not available

and increasing subbottom depth with increasing water depth. The exact formation of the hydrate, however, is still controversial and different models have been proposed to explain the origin of BSRs (Hyndman and Davis, 1992; Kvenvolden and Barnard, 1983a).

One of the first regions where a bottom simulating reflection was detected and related to the occurrence of methane hydrate is on the eastern United States margin, offshore Florida, on the Blake Outer Ridge. Deep-sea drilling on the Blake Outer Ridge found high methane content which suggested that the reflection was associated with the presence of methane hydrate (Shipley et al., 1979). Based only on apparently high velocities in the sediments of the ridge, Bryan (1974) explained the reflection by gas accumulation at the base of the hydrate zone.

In this study, we use the AVO amplitude responses and impedance estimates of marine seismic data recorded at the Blake Outer Ridge to explain the present bottom simulating reflection and to explore the validity of the different origin models. By doing this detailed AVO analysis we can clearly discriminate the effects of the two proposed BSR models. The variation of amplitude versus offset can be an important indicator of free gas at an interface (Shuey, 1985) and, together with the estimation of material properties at the interface, limits the possible explanations of the physical origin of the BSR considerably.

This paper discusses our work with preprocessing, inversion and interpretation of the methane hydrate seismic data. The data are preprocessed by first applying a spherical divergence correction. Then a source wavelet deconvolution followed by an NMO correction and amplitude calibration are performed. The deconvolution and amplitude correction serve as a receiver compensation for the group array response. To account for the use of a non-linear streamer during the recording, the data are then linearly interpolated at the near offsets. A velocity analysis is performed on the resulting data and they are again processed with an additional static shift to improve the NMO correction. Using the observed AVO curves at the reflectors, the P and S impedance contrasts are estimated and used in a preliminary interpretation of the data.

METHANE HYDRATE AND BSRS

A methane hydrate is an ice-like, crystalline lattice of water molecules in which gas molecules are trapped physically without the aid of direct chemical bonds. It forms only under certain pressure and temperature conditions (Figure 1) which restrict the BSRs to two regions: polar and deep oceanic. In polar regions, the BSRs are normally associated with permafrost both onshore in continental sediment and offshore in sediment of the continental shelves. In deep oceanic regions, BSRs are found in outer continental margins in sediment of slopes and rises where cold bottom water is present.

Two models have been proposed to account for gas hydrate formation and the

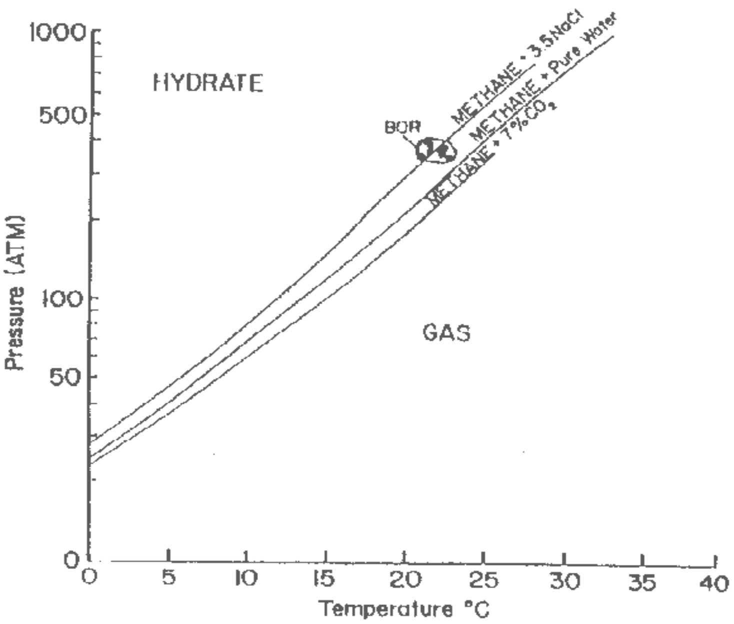

Figure 1: Pressure-Temperature relation for hydrate stability at different compositions. BOR indicates the conditions at the Blake Outer Ridge. christin-hydrate [NR]

development of BSRs. In the first, methane is assumed to be generated locally from organic material at the depth of the hydrate. As the zone of methane hydrate thickens and deepens, its base eventually subsides into a temperature region where the hydrate is unstable. In this region free gas can occur (Kvenvolden and Barnard, 1983a). As a consequence, the BSR is caused by the impedance contrast at the base of the hydrate layer and top of the gas layer. The second model assumes that the methane hydrates are formed through the removal of methane from rising pore fluids being expelled upwards from deeper in the sediment section (Hyndman and Davis, 1992). Most of the methane is generated at depths below the hydrate stability zone but not at depths sufficient for the formation of thermogenic methane. Therefore, the methane hydrates should be concentrated at the base of the stability zone and free gas does not have to be present below the BSR. In this case the BSR is the consequence of the impedance contrast between overlying sediments containing substantial amounts of high-velocity hydrate and underlying normal velocity brine sediments.

The approximate AVO amplitude responses of these BSR reflection models, based on linearized Zoeppritz reflection coefficients, are shown in Figure 2.

A transition from overlying sediment containing methane hydrate to sediment containing free gas, having a low Poisson's ratio, gives a large decrease in Poisson's ratio and thus reflection amplitudes increase rapidly with increasing angle. On the other hand, sediment containing methane hydrate overlying brine sediment does not much change the amplitude with increasing offset. A comparison between this ex-

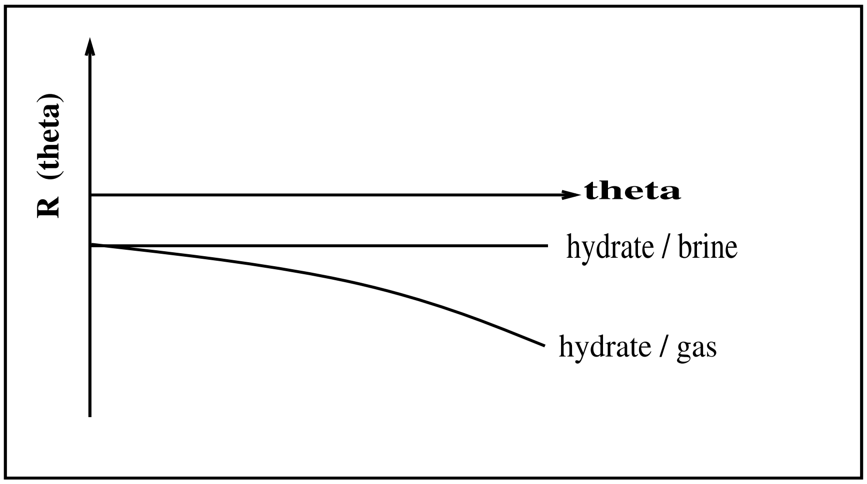

Figure 2: Expected BSR AVO curves for hydrate overlaying brine sediment, and hydrate overlaying free methane gas. christin-avo [NR]

pected behavior with the one observed in this study should give a first order insight into the possible origin of the BSR in the data.

BLAKE OUTER RIDGE SEISMIC DATA

The seismic data used for this study consist of 201 CMP gathers recorded along the Blake Outer Ridge with a non-linear streamer resulting in a 100 m group spacing at the near offset traces and a 50 m group spacing at the far offset traces (Figure 4).

The seafloor reflection occurs at about 4.4 seconds, indicating a water depth of over 3 km, and decreases in depth gradually along the line (Figures 4 and 3). It is followed by a strong bottom simulating reflection at approximately 5.2 seconds vertical traveltime. A fairly bright "flat spot" reflection is apparent beneath the BSR at 5.4 seconds, which does not parallel the seafloor or BSR reflection events. Examining the raw prestack data, a traveltime kink is very striking in all reflections near the central offset of the CMP gathers. This kink occurs exactly at the transition zone between the nonlinear cable group spacing of 100 m at the near offsets, and 50 m group spacing at the far offsets. Adding the far offset traces in pairs to simulate a constant cable group spacing of 100 m at all offsets eliminates the traveltime kink in the data (Figure 5), but causes adverse waveform and amplitude changes with offset.

The group-corrected data have less spatial resolution than the original data, based on a decrease from 48 to 36 traces. Furthermore, the group summation causes a significant loss in temporal frequency content at the far offsets, due to spatial averaging of moveout delayed reflections across a twice longer effective group array. One possibility to compensate for this low frequency group array response is to filter (deconvolve) the far offset data in the k-x domain. However, the decreased number of summed far

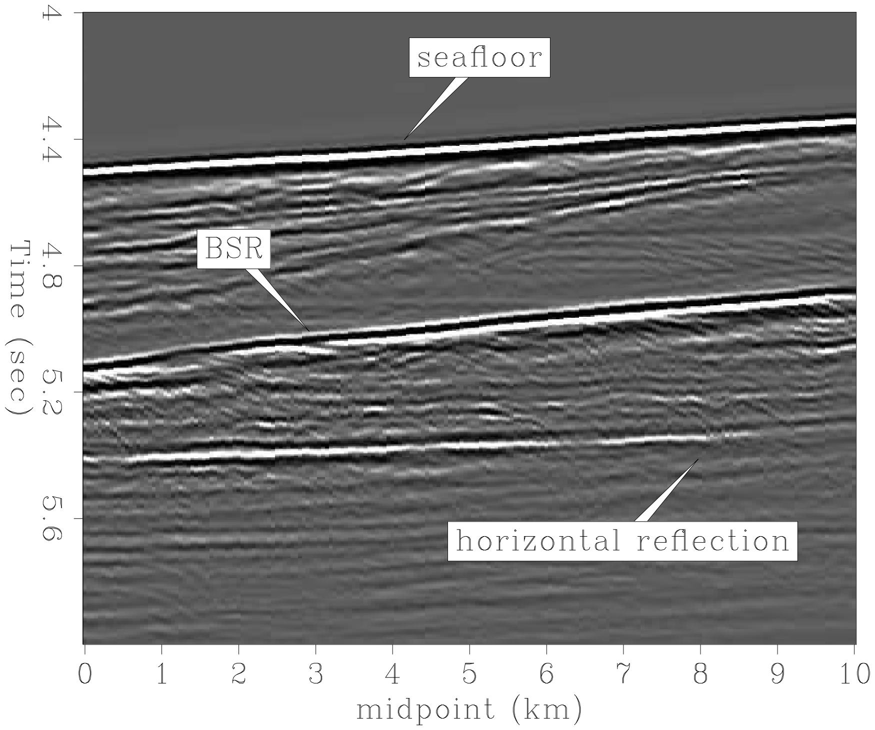

Figure 3: Stacked section. christin-stack-ann [ER]

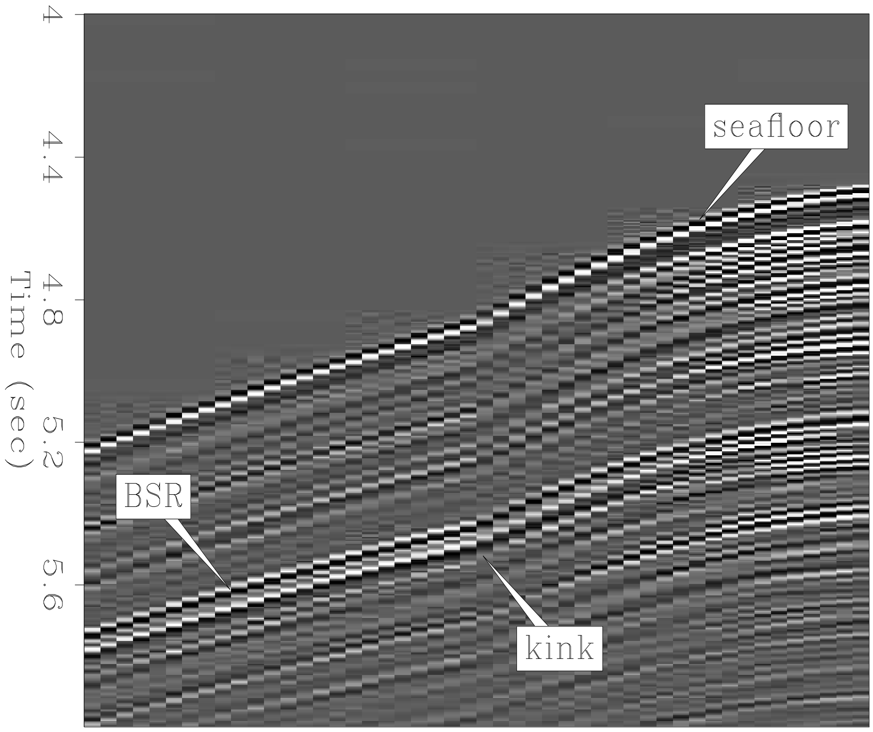

Figure 4: A raw CMP gather. christin-cmp1-ann [ER]

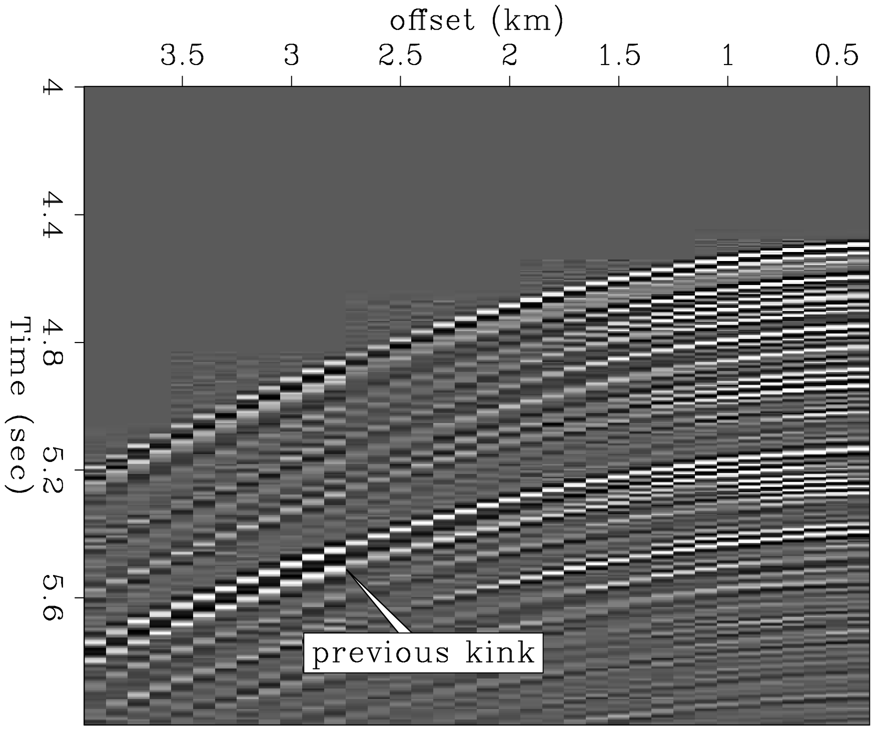

Figure 5: CMP gather with a constant group spacing of 100 m at all offsets. christin-cmp2-ann [ER]

offset traces result in a very short data series, which makes accurate spectral estimates and the application of spatial deconvolutional filters difficult. Another possibility to account for this frequency loss is to deconvolve the far offsets as function of the Snell parameter p in the slant stack domain. Unfortunately, the small number of traces tends to introduce large edge effects in the slant stack spectrum. These edge effects could be minimized by using a least-squares slant stack which, however, would smear the notches in the $\tau - p$ spectrum, and the resulting deconvolution would overemphasize those portions of the spectrum. Therefore, it seems unreasonable to correct the raw data for the different group spacings by summing the far offset traces in pairs. A simple linear interpolation of the near offset traces after NMO, with source wavelet deconvolution and amplitude calibration to compensate for the group array response appears to be a better method for suppressing the nonlinear cable effects.

PROCESSING STEPS

Preprocessing and velocity analysis

In the first preprocessing step, the raw data were corrected for constant velocity spherical divergence by multiplying each trace with a time-variant amplitude scale function of the form $A(t) = t$. Following the divergence correction, we performed a normal moveout correction with an initial estimate of the best stacking velocity function. A windowed section of the first CMP gather can be seen in Figure 6.

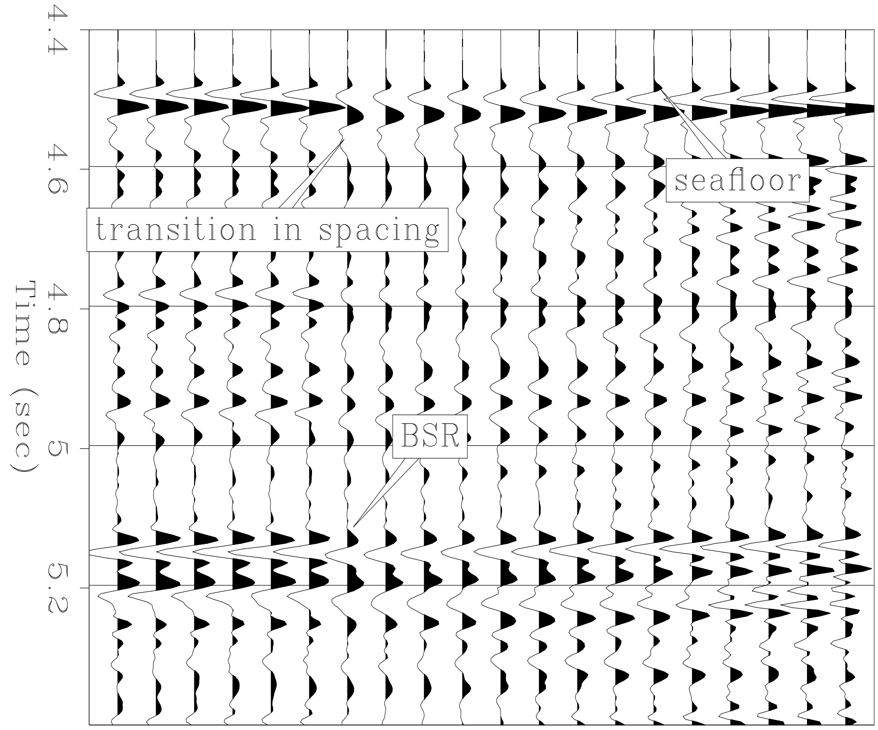

Figure 6: CMP gather after NMO correction. christin-nmo-ann [ER]

A significant change in shape and amplitude of the source wavelet is visible at the transition zone between the 50 m and 100 m group spacings, where the wavelet exhibits very low frequency content and weak amplitude. In the direction of the near offsets (to the right in Figure 6), the wavelet sharpens again and regains its large amplitude. These waveform shape and amplitude changes with offset can seriously degrade any subsequent AVO analysis. In order to regularize the wavelet as much as possible, a single trace source wavelet deconvolution before NMO correction was performed. Although the application of single trace, as opposed to surface-consistent, deconvolution can result in undesired changes in amplitude and waveform, the Blake Outer Ridge seismic data were of high enough quality that single trace deconvolution with careful quality control gave very consistent results. The deconvolved data were then bandpass filtered to the original data bandwidth to remove spurious deconvolutional high frequency noise, and again NMO corrected. After having accounted for the change of the waveform shape at the transition zone, the amplitude change also required compensation. In order to do this, two main assumptions were made. First, it was assumed that an offset-dependent rather than an angle-dependent amplitude correction was sufficient, since the difference between the maximal angle of incidence at the seafloor (33°) and the BSR reflection (30°) is negligibly small. Second, we assumed a functional form for the AVO response of the seafloor reflection, based on equal positive P and S impedance contrasts, adjusted here to 0.4 respectively, via linearized Zoeppritz modeling. Based on these assumptions, the amplitude calibration was performed by scaling each trace to the seabottom amplitude to match the predicted seafloor AVO, as a function of offset. Figure 7 shows a windowed CMP section after the deconvolution and amplitude corrections.

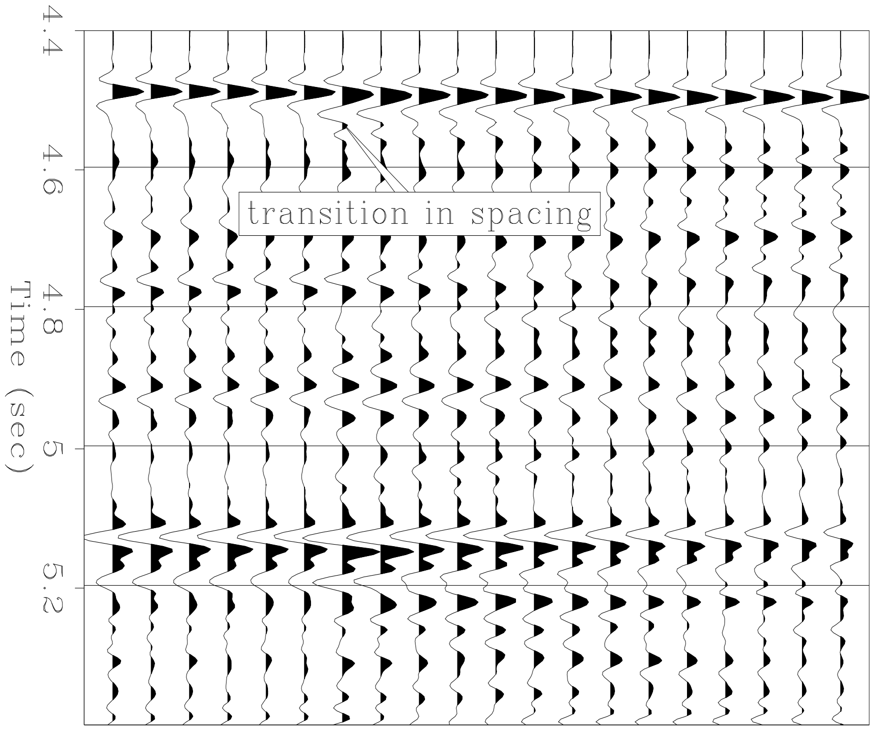

Figure 7: CMP gather after deconvolution and NMO. christin-nmo-corr-ann [ER]

Comparing this result with the previous figure, the improvement of the waveforms is obvious. There are only small variations in the shape of the wavelet left and the amplitudes are physically consistent across the entire offset range.

A linear interpolation at the near offsets was used to even the group spacings to 50 m at each offset and thus eliminated the traveltime kink introduced by the nonlinear streamer. After applying an inverse NMO correction to the interpolated data, a high resolution NMO stacking velocity analysis was performed. The velocity scans showed a nearly linear rms velocity function at each CMP, which varies as a function of depth below the seafloor (Figure 8). A 2-D rms velocity model was built based on the velocity scan information along the line. It assumes a water velocity of 1.48 km/s and increases linearly with depth with a constant gradient of 0.06 km/s/s (Figure 9).

After having derived a good stacking velocity model for the data, they were processed again by using the new velocity model. Since it is essential for the subsequent impedance contrast estimation that the reflector moveout is very flat after NMO correction, an additional static shift was applied before the amplitude scaling to correct for some small non-hyperbolic offset-dependent moveout in the CMP gathers. The fi-

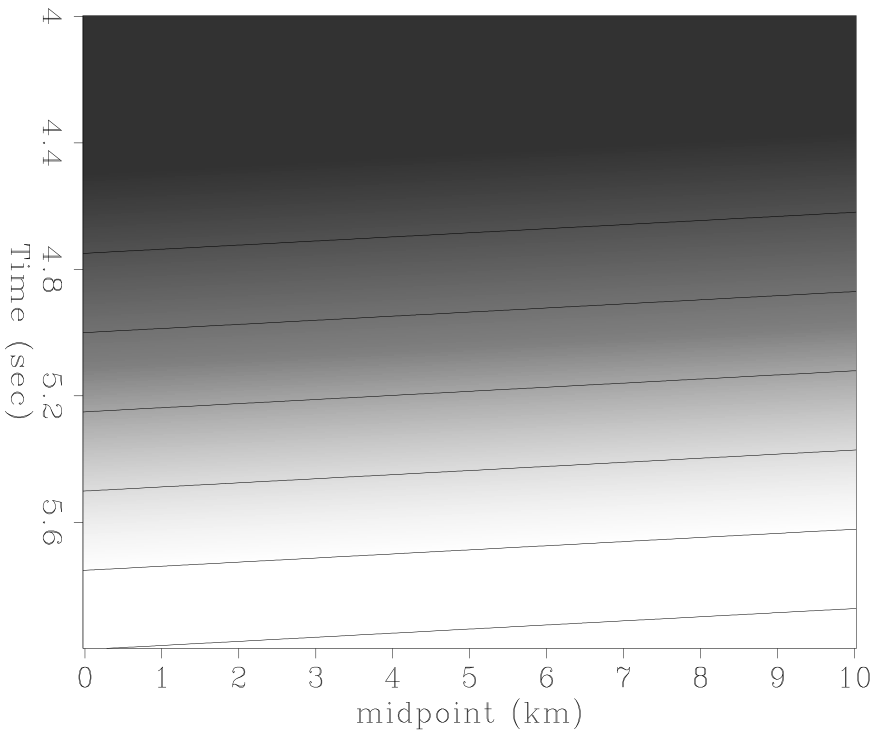

Figure 8: 2-D rms velocity model. $\boxed{\text{christin-2Dvel}}$ [ER]

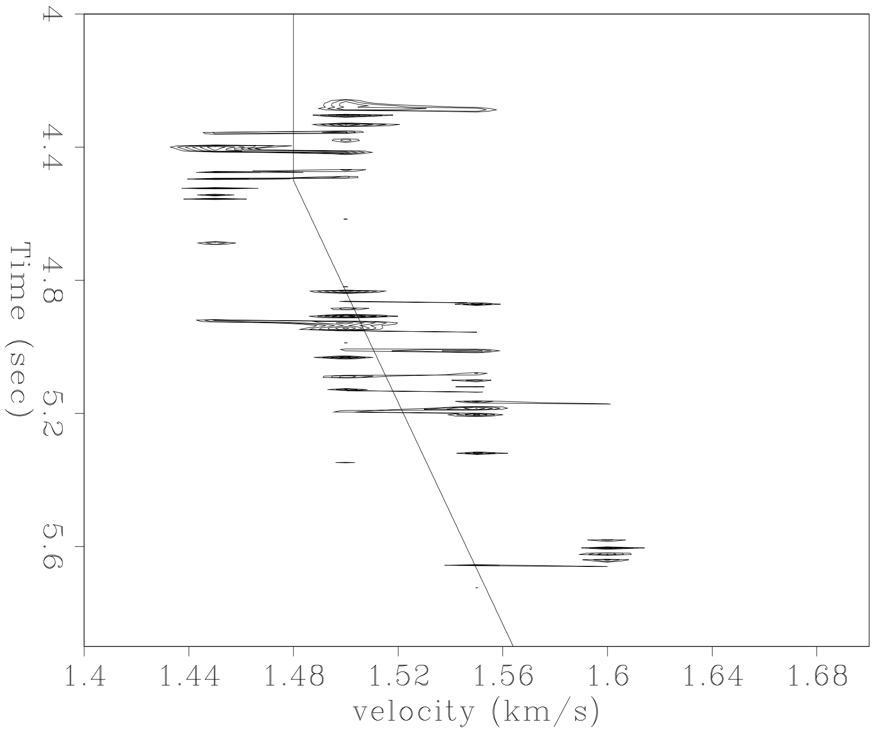

Figure 9: Linear rms velocity model overlain on its respective NMO velocity scan. $\boxed{\text{christin-velo}}$ [ER]

nal deconvolved, NMO, static, amplitude and group spacing corrected data are shown in Figure 10.

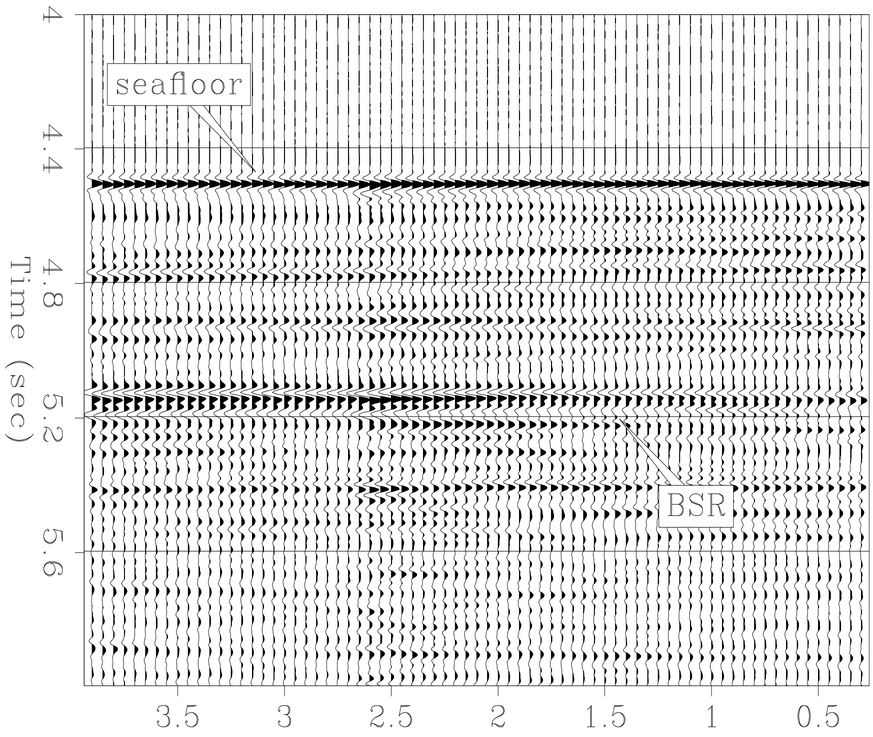

Figure 10: Final CMP gather after deconvolution, NMO, amplitude correction and linear interpolation to account for the variable group spacings. christin-int-ann [ER]

This figure clearly indicates the nearly constant AVO amplitudes of the seafloor reflection and the increasing negative amplitudes with increasing offset of the hydrate reflection. This result can be compared with the theoretical AVO curves for hydrate over sediment and hydrate over gas which were shown in Figure 2. The comparison of the observed behavior with the predicted one already suggests that there might be free gas present beneath the bottom of the hydrate stability field.

Impedance contrast estimation

The P and S impedance contrasts at each subsurface position were then estimated by applying a least squares elastic parameter inversion method (Lumley and Beydoun, 1991; Lumley, 1993) to the preprocessed CMP gathers. This technique fits the observed AVO curves of the reflectors at each pseudo-depth and surface position to the theoretical P and S impedance curves (Figure 11) which are based on linearized Zoeppritz equations.

For a unit perturbation in relative P impedance contrast, the P impedance inversion curve dominates at small angles of incidence and increases with increasing angles of incidence. For a unit perturbation in relative S impedance contrast, the S

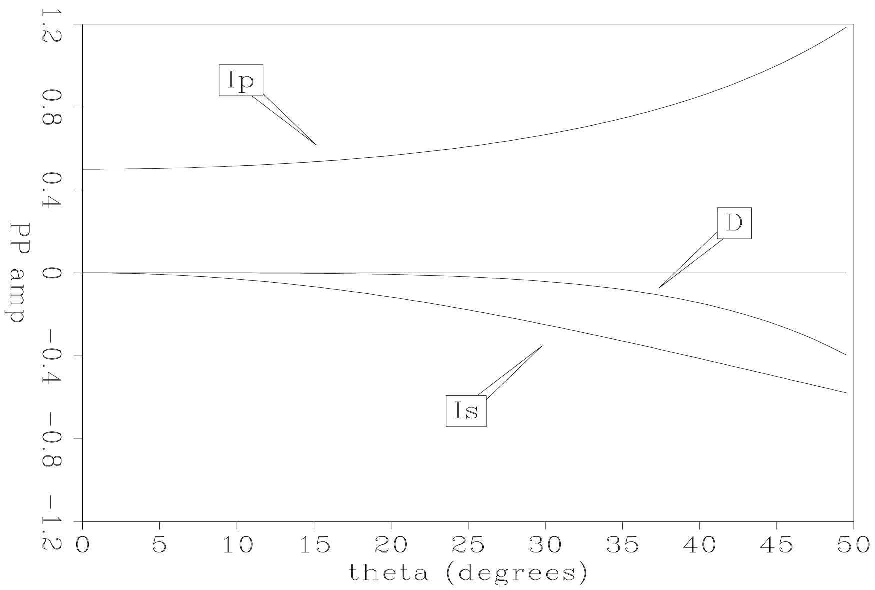

Figure 11: Theoretical P, S and density impedance inversion curves. christin-imped [NR]

impedance inversion curve is zero at normal incidence, and is increasingly negative with increasing offset. Over the conventional range of surface reflection data acquisition geometry illumination, which is typically 0° to 35°, the density inversion curve is not significant, as most of the density contrast contributes to the reflection AVO through the impedance contrasts alone. As the reflection amplitudes are mostly a combination of the P and S impedance contrast inversion curves, reflectors with P and S impedance contrasts of the same polarity and magnitude are expected to show approximately constant amplitudes versus offset. On the other hand, reflectors with P and S impedance contrasts of opposite polarities, indicating a transition zone of changing rock pore fluid properties, should show either increasing positive or increasing negative amplitude versus offset. The least-squares impedance inversion results of the preprocessed CMP gathers are shown in Figures 12 and 13.

RESULTS

The P impedance contrast section shows clearly that the seafloor reflection and BSR have P impedance contrasts of opposite polarity. In a small section right above the BSR, there is a "quiet" zone where no diffractions or reflections are visible. Below the BSR a horizontal reflector gives a strong impedance contrast of the same polarity as the seafloor. The S impedance contrast section is dominated by a lot of diffraction signals, since the data are unmigrated. The seafloor has a much weaker shear impedance contrast than the BSR, but it is evident that both have the same polarity. The horizontal reflector below the BSR nearly disappears in this section suggesting that this transition zone has a very small S impedance contrast. A simple multiplica-

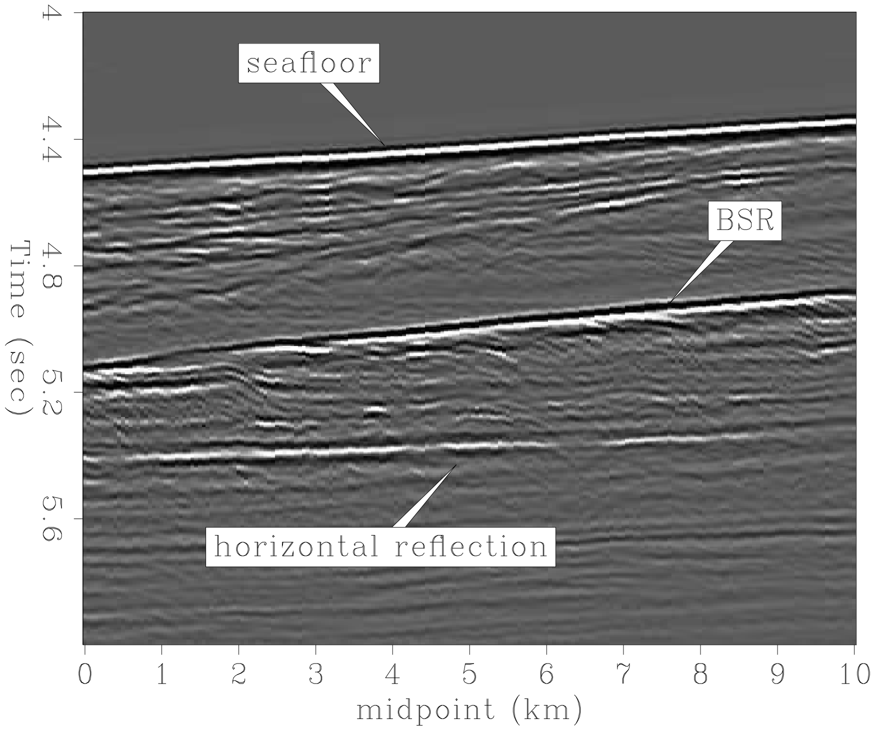

Figure 12: P impedance contrast christin-pmp-ann [ER]

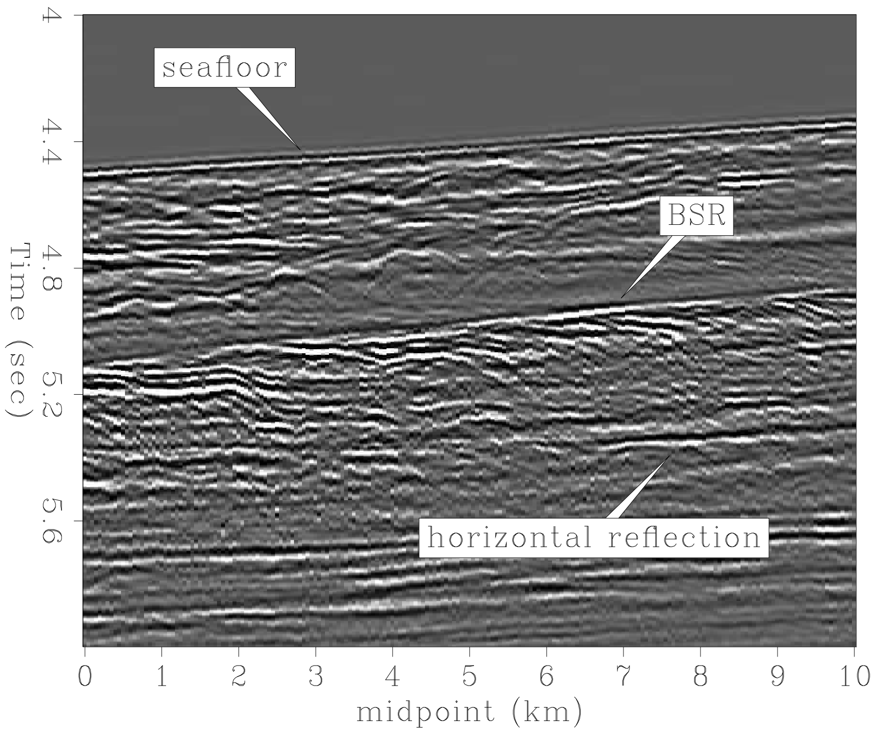

Figure 13: S impedance contrast christin-smp-ann [ER]

tion of the P and S impedance contrast sections produces a P*S anomaly map shown in Figure 14. P and S impedance contrasts of the same signs are plotted dark grey, contrasts of opposite signs are plotted white.

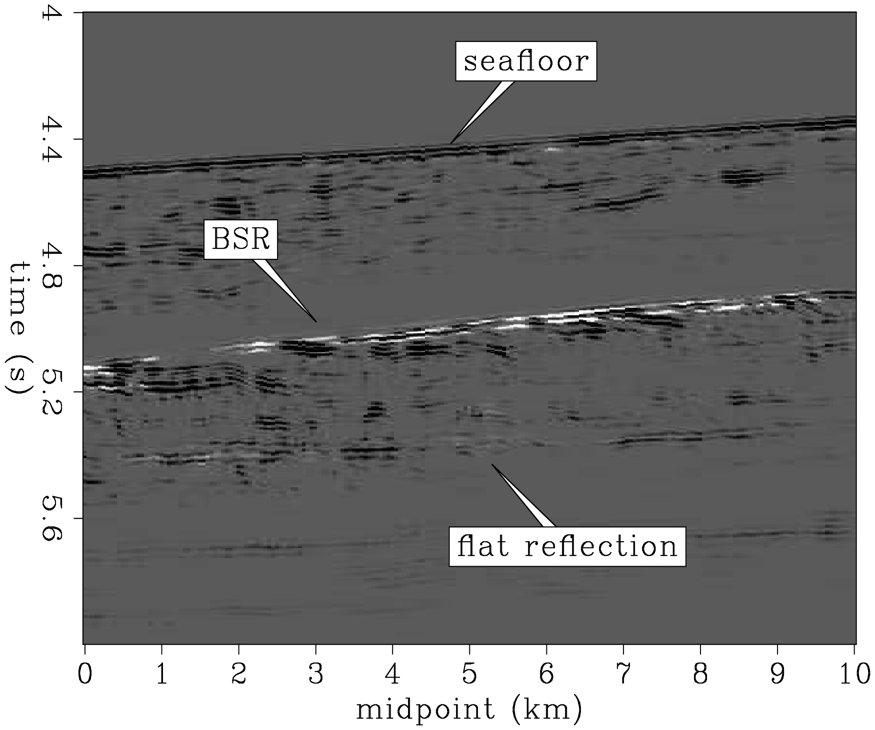

Figure 14: P*S impedance contrast. christin-PSmap-ann [ER]

Having a calibrated amplitude AVO response, the seafloor results show an equal magnitude, positive P and S impedance contrast. The BSR has clearly opposite P and S impedance polarity. From the AVO amplitude responses it is known that the amplitudes of the BSR increase negative with increasing offset. This means that the reflector has a positive S and negative P impedance contrast. A hydrate-gas transition would explain such P and S impedances, whereas a hydrate-brine transition zone can be expected to have both negative P and S impedances. Thus, the presence of free gas below the BSR seems to be indicated. The "quiet" zone above the BSR where no reflections or diffractions can be seen might be explained by the presence of disseminated methane hydrate. Assuming that the BSR is associated with the base of the methane hydrate stability field, the hydrate accumulates right above the BSR and diminishes gradually with increasing height. The ice-like particles behave like small point scatterers for an incident seismic signal and mask each other. The bright reflector beneath the BSR has a positive P impedance contrast and may have a negative S impedance contrast, although the signal is quite weak. This could indicate a reflection at the bottom of the free methane gas layer overlying normal brine-saturated sediments. Such a transition zone has a positive P impedance contrast and a small, if any, positive S impedance contrast. Furthermore, a gas-water contact is likely to give a horizontal reflection as the base of gas is not following a pressure-temperature boundary but is controlled by gravity. Such horizontal reflectors are usually known as flat spots, and are often found to correlate with gas-fluid contacts.

Assuming a seafloor reflection coefficient of 0.2 and fixing the P and S impedance contrasts of the seafloor to 0.4 each, it is possible to estimate the relative impedance contrasts of the BSR by determining the average amplitude changes between seafloor and BSR. This results in a P impedance contrast of -0.4 which has the same magnitude but opposite polarity to the seafloor. The S impedance contrast is very strong and amounts to approximately 0.8 to 1.2 which is two to three times as much as the seafloor impedance contrast of the same polarity. This high magnitude has the effect of visually diminishing the S impedance contrast of the seafloor (Figure 13) compared with the P impedance contrast (Figure 12) which actually are scaled to be the same.

Given the stacked section of the processed data (Figure 15), the geology was interpreted using the impedance inversion results (Figure 16). The water bottom overlays marine sediments that gradually accumulate into methane hydrate with depth. Since the transition is gradual, it can not be seen as reflections in the data. The hydrate zone may be characterized by many small ice diffractors which eliminate each other effects and create a seismic "quiet" zone. The bottom of the methane hydrate gives a strong reflection of negative polarity. Based on the impedance contrasts and AVO amplitude responses, the hydrate is assumed to overlay sediments in which free gas is trapped. The flat reflector below the BSR could correspond to a gas-water contact, but has to be investigated in more detail before a final interpretation can be made.

Future work

After having performed a conventional AVO analysis on the data, the following steps will be done next:

- prestack migration before AVO
- finite difference modeling

CONCLUSIONS

A detailed AVO analysis was performed on data from the Blake Outer Ridge to evaluate the origin of the bottom simulating reflector. We could clearly discriminate the effects of the two proposed models and showed that the BSR best fits a model of impedance contrasts between sediments containing a substantial amount of hydrate overlaying sediments containing free gas. A transition from hydrate to brine sediments is not consistent with the AVO amplitude responses and impedance contrasts. Assuming a reflection coefficient of 0.2 at the seafloor, the P impedance contrast at the BSR could be determined to -0.4. It has the same magnitude but opposite polarity to the seafloor impedance contrast. The resulting S impedance contrast of

0.8-1.2 at the BSR is two to three times larger than the seafloor S impedance contrast of the same polarity. A horizontal reflector below the BSR might be a "flat" spot which separates the free gas trapped below the BSR from deeper sediments saturated with water. However, this flat spot interpretation is so far inconclusive. A prestack migration impedance inversion might clarify the flat spot properties.

ACKNOWLEDGMENTS

We thank Keith Kvenvolden, Bill Dillon and Myung Lee of the USGS for providing us with a copy of the Blake Outer Ridge seismic data used in this study.

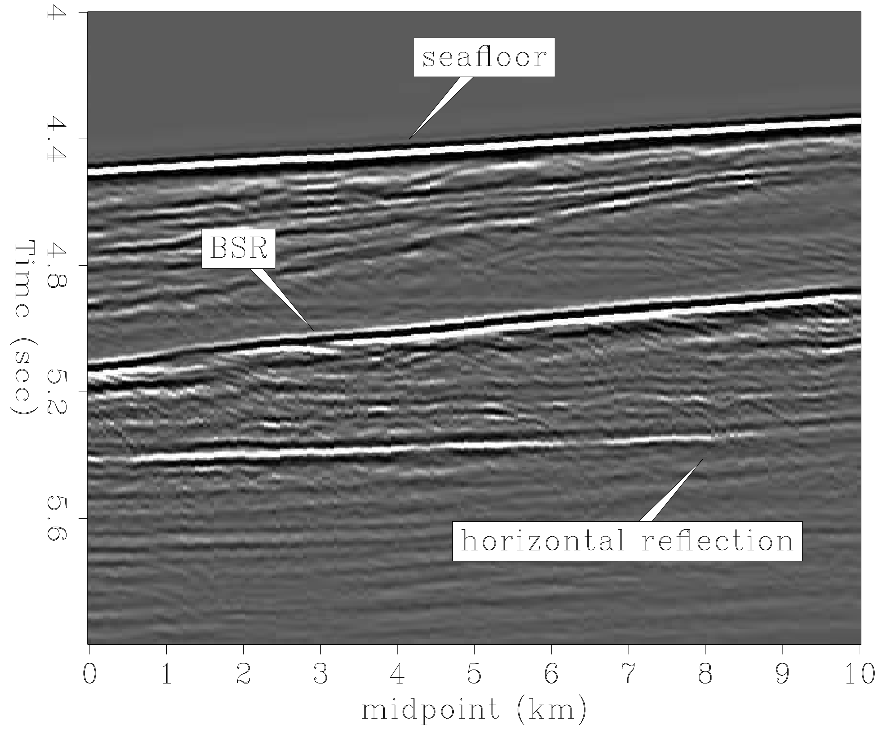

Figure 15: Stacked section. christin-stack2-ann [ER]

REFERENCES

Bryan, G. M., 1974, In situ indications of gas hydrate: Marine Sciences, **3**, 299–308.

Hyndman, R., and Davis, E., 1992, A mechanism for the formation of methane hydrate and seafloor bottom simulating reflectors by vertical fluid expulsion: J. Geophys. Res., **97**, 7025–7041.

Hyndman, R., and Spence, G., 1992, A seismic study of methane hydrate marine bottom simulating reflectors: J. Geophys. Res., **97**, 6683–6698.

Kvenvolden, K. A., and Barnard, L. A., 1983a, Hydrates of natural gas in continental margins: Am. Assoc. Pet. Geol. Mem., **34**, 631–640.

Kvenvolden, K., 1993, Gas hydrates – geological perspective and global change: Reviews of Geophysics, **31**, 173–187.

Lumley, D., and Beydoun, W., 1991, Elastic parameter estimation by Kirchhoff prestack depth migration inversion: SEP–**70**, 165–192.

Lumley, D. E., 1993, Kirchhoff prestack impedance inversion: A gas reservoir pilot study: SEP–**77**, 211–230.

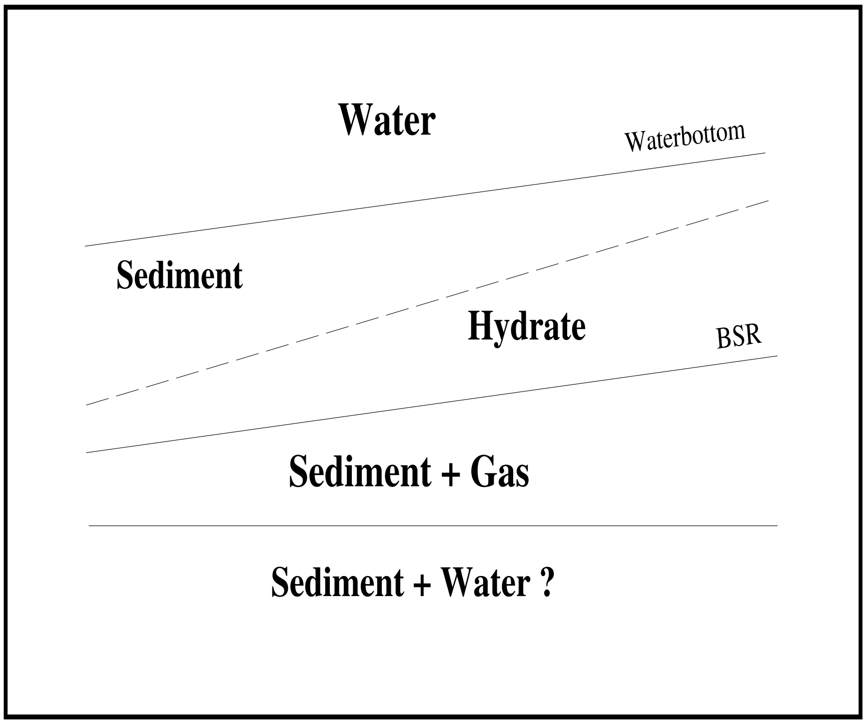

Figure 16: Preliminary interpretation of the methane data. christin-interp [NR]

Miller, J. J., Lee, M. W., and vonHuene, R., 1991, An analysis of a seismic reflection from the base of a gas hydrate zone , offshore Peru: Am. Assoc. Pet. Geol. Bull., **75**, 910–924.

Shipley, T. H., Houston, M. H., Buffler, R. T., Shaub, F. J., McMillen, K. J., Ladd, J. W., and Worze, J. L., 1979, Seismic evidence for widespread possible gas hydrate horizons on continental slopes and rises: Am. Assoc. Pet. Geol. Bull., **63**, 2204–2213.

Shuey, R. T., 1985, A simplification of Zoeppritz equations: Geophysics, **50**, 609–614.

Singh, S., Minshull, T. A., and Spence, G., 1993, Velocity structure of a gas hydrate reflector: Science, **260**, 204–207.